The International Journal of Advanced Manufacturing Technology (2024) 130:1355–1371
https://doi.org/10.1007/s00170-023-12744-9

ORIGINAL ARTICLE

Comparison of laser shock dynamic compaction with quasi-static compaction

Tao Wang[1] · Maomao Cui[1] · Zhao Zhang[1] · Huixia Liu[1] · Youjuan Ma[1] · Wenkai Shen[1] · Xiao Wang[1]

Received: 15 August 2023 / Accepted: 25 November 2023 / Published online: 9 December 2023

Abstract

By combining the distinctive advantage of the pulsed laser with a high strain rate, this study conducts dynamic compaction experiments with high-strain rate laser shock and quasi-static compaction with a low strain rate on aluminum-based composite powder (Wp/Al) and analyzes the effects of pressing pressure and Wp content on the relative density, surface microstructure, demolding pressure, radial rebound, and mechanical properties of Al-based composite (Wp/Al) compacts under the two modes of action. The shock wave propagation process, densification process, and adiabatic temperature rise in the pressed billet at high strain rates due to laser shock are analyzed in combination with 2D MPFEM. Results show that the relative density of the billets decreases as the Wp particle content increases and that the relative density of the billets obtained with high-strain rate laser shock dynamic compaction is 97.62%, which is up to 2.9% higher than that of quasi-static compaction with low strain rate, the demolding pressure decreases by up to 1.56 times, and the hardness increases by up to 13.5%. The hard particles Wp are evenly distributed on the surface of the billet, and no significant aggregation of hard particles is observed. The 2D MPFEM reveals that the speed between particles within the powder at the beginning of the pressing reaches the minimum collision speed of welding, which is beneficial to the particles to achieve improved adhesion; laser high-speed impact under the particles due to inertial effects produces severe plastic deformation, which in turn improves the formability of the powder; in the process of laser shock the temperature at the edge of the particles is greater than the temperature inside the particles, and the temperature near the upper impactor is higher. In addition, the results of the simulation study are compared with the experiments and are found to be remarkably consistent.

Keywords Laser shock · Dynamic compaction · 2D MPFEM · Compound powder · Enhancement phase

1 Introduction

Powder metallurgy is one of the most commonly used methods for producing high-quality, high-precision, and near-net-shaped [1] structural parts, and the powder compaction process is a crucial step in powder metallurgy to obtain powder metallurgical parts with excellent performance. To develop an efficient powder compaction process for the production of high-density and high-performance compacted blanks, the main powder compaction processes are currently classified as quasi-static compaction, high-speed compaction (HVC), and dynamic compaction. Although isothermal static pressing and hot pressing can be used to improve the densities of the pressed billets, the costs are too high. HVC improves the densities and mechanical properties of the pressed billets in comparison with quasi-static compaction, and researchers have focused on the effects of parameters such as peak pressure [2, 3], impact velocity [4, 5], impact energy [6–9], and several impacts [10] on the relative density and mechanical features of the pressed billets, where green powders can be instantly densified by one or more high-energy impacts [10], which reduce the rebound of the billet [11] and broaden the range of materials to be pressed [6]; however, the pressing speed of HVC is in the range of 3–20 m/s, which makes it difficult to increase the densification of the billet further. Dynamic compaction mainly includes electromagnetic pulse dynamic compaction and explosive compaction. Compared with high-speed compaction, which has been greatly improved, the powder under high-speed impact produces high-strain-rate plastic deformation, thus further improving the compacted billet density and mechanical properties

---

✉ Huixia Liu
lhx@ujs.edu.cn

[1] School of Mechanical Engineering, Jiangsu University, Zhenjiang 212013, China

[9]. Dong et al. [12, 13] conducted an experimental study of the dynamic compaction of Cu powder using the magnetic pulse dynamic compaction (MPC) technique, resulting in a maximum relative density of 96% for Cu powder billets; however, the results showed an uneven distribution of microhardness between the upper and lower faces of the billets and a slight delamination of the lower face of the billets. Atrian et al. [14] conducted dynamic compression tests on SiC-reinforced Al7075 metal matrix composites using a split Hopkinson pressure bar (SHPB) at different strain rates. Composite powder compacts of Φ15 mm × 8 mm were successfully produced, but the agglomeration of nanoparticles (SiC) resulted in stress concentration and nonuniform density spread in the pressed billets. Sharma et al. [15] dynamically compacted Cu powder using different blast speeds, resulting in miniature Cu pressed billets with a relative density of 94% and good microhardness, but the operability and reliability of the procedure still need further improvement. Therefore, on the basis of the above analysis, a new powder compacting process suitable for the dynamic compaction of micro parts must be developed urgently.

Given the pulsed laser's ability to generate shock waves with high strain rates (10^6–10^7 s^{-1}), the energy can be applied to the powder and compacted rapidly in a short period. The laser has also been widely used in micro-forming due to its controlled energy and smaller area of action [16–19]. This group proposed a new approach of laser dynamic shock compaction based on the distinctive advantages of a pulsed laser with high-strain rate dynamic loading features that is suitable for micro-forming [20]. Ni et al. [20] successfully produced Φ2.5 mm × 0.5 mm pure Al powder pressed billets with a density of 99.72% using the laser shock dynamic compaction technique. Wang et al. [21] successfully manufactured tungsten carbide particle (WCp) reinforced Al matrix composites (WCp/Al) using a high-strain rate laser impact dynamic compaction technique, with a relative density of 97.72% in the final compacted billets. To highlight the advantages of the laser impact dynamic compaction procedure, this study compares the laser shock dynamic compaction process with the quasi-static compaction procedure. Experiments on high-strain-rate-laser shock dynamic compaction and low-strain-rate quasi-static compaction of aluminum-based composite powder (Wp/Al) must be conducted, and a comparative study must be performed to analyze the effects of compaction pressure and Wp content on the relative density, surface microstructure, molding pressure, radial rebound, and mechanical properties of Al-based composite (Wp/Al) compacts under the two modes of action. The analysis of shock wave propagation, densification procedure, adiabatic temperature rise, and inertia effect under laser shock dynamic compaction was also studied in combination with 2D MPFEM to reveal the compaction characteristics of laser shock dynamic compaction of composite powders.

2 Experimental procedures and methods

2.1 Experimental principles

Figure 1 displays the principle diagram of the laser shock dynamic compaction experiment, which includes two parts: the mold and pulsed laser. The laser is controlled by a computer to generate different laser energies, and the laser beams with different laser energies are reflected onto the focusing lens through the reflecting mirror surface, which eventually

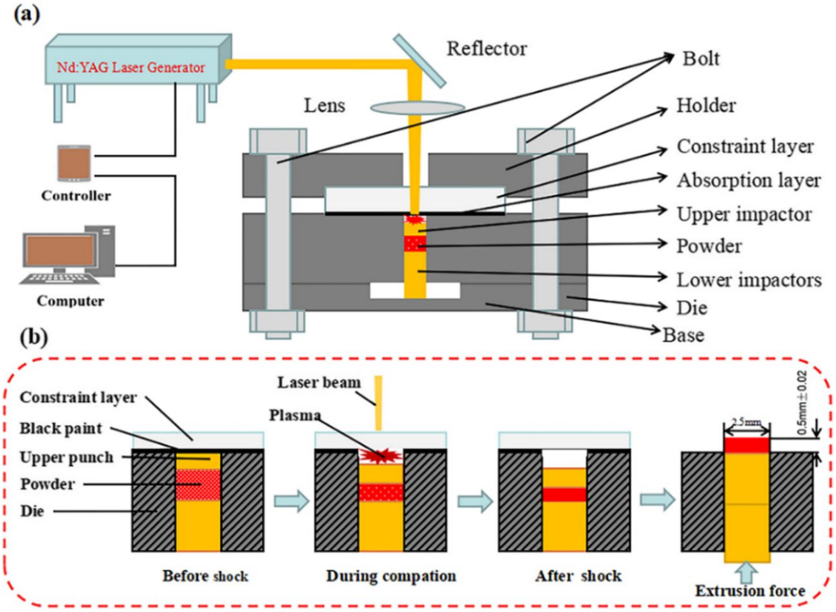

Fig. 1 Demonstration of the principle of the laser shock procedure: **a** assembly diagram of the laser shock working principle, **b** laser shock composite powder compaction process

forms a circular spot size on the absorption layer. The Nd-YAG pulsed laser was used for this experiment. A 2.5 mm spot diameter was used for the laser, the pulse duration of the laser was 8 ns, the wavelength was 1064 nm, and the maximum pulse energy was 1800 mJ. Figure 1a shows the composition of the mold for this experiment. Figure 1b shows a schematic diagram of the laser shock procedure. By the laser emitting laser radiation on the black paint, the black paint explodes in a short time (1 µs) to generate a high-pressure plasma blast wave acting on the surface of the upper impactor, driving the upper impactor to compact the composite powder quickly.

2.2 Experimental materials and methods

2.2.1 Experimental materials

The tungsten powder used in this experiment was provided by Nangong Xindun Alloy Welding Spraying Co., Ltd., and the pure Al powder was provided by Beijing Gaoke New Material Co., Ltd. Table 1 shows the specific material parameters. Figure 2a displays the microscopic shape of aluminum powder, and Fig. 2b displays the microscopic shape of Wp. As shown in the figure, the Al powder and Wp are approximately spherical, the particle size of aluminum powder is approximately 20 µm, and the particle size of tungsten powder is approximately 3 µm. During the blending process, the composite (Wp/Al) mixture is suspended in ethanol and subjected to 20 min of ultrasonic shaking to prevent agglomeration of the Wp. The neutral environment of ethanol prevents the oxidation of the Al particles. After drying, the mixture was ground with 0.5 wt% stearic acids in a star ball mill (speed 300 r/min) under argon gas to disperse the Wp uniformly over the surface of the Al particles.

Table 1 Specific technical parameters of pure aluminum powder and Wp

Powder	Grade	Particle size (µm)	Purity (%)	Tap density (g/cm^3)	Theoretical density (g/cm^3)
Al	3N	20	> 99.9%	30%	2.78
Wp	–	3	> 99.9%	23%	19.35

2.2.2 Experimental setup and parameters

CNC press (UTM4104, SHENZHEN) was used for quasi-static compaction in the experiments, and Fig. 3a shows the variation curve of pressure with time during the experimental process, while Nd-YAG pulsed laser was used for the laser in the experiments, and Fig. 3b shows the variation curve of the stress wave with time during the dynamic compaction process of laser shock. For the laser shock dynamic compaction experiments, the constrained layer (PMMA) with black paint sprayed on the lower surface is held in place by a pressing device, the depth of the black paint is approximately 50 µm, and the upper and lower impactors are gap-fitted to the powder cavity to reduce the effect of air resistance. All parts are secured by bolts with a guaranteed preload to prevent leakage of plasma gas from the explosion. Table 2 shows the specific workpiece parameters. Prior to the laser shock dynamic compaction experiments, composite powders (Wp/Al) with different tungsten powder contents (5%, 10%, 15%) were pre-pressed on a CNC press and respectively compacted into certain shapes to facilitate the subsequent filling steps, so that the initial relative density of the pressed billets reached about 55%, and in order to measure the true density of the pressed billets, the Archimedes principle was used to measure the density of each pressed billet. In the laser dynamic compaction experiments, five different laser energies (600, 900, 1200, 1500, 1800 mJ) were chosen for the experiments and to ensure the credibility of the results each set of experiments was repeated at least three times. A tungsten filament scanning electron microscope (SEM, Hitachi S-3400 N) was used to observe the surface microstructure of the composite powder press billets. The microscopic microhardness distribution of the composite powder pressed billets with different Wp contents was

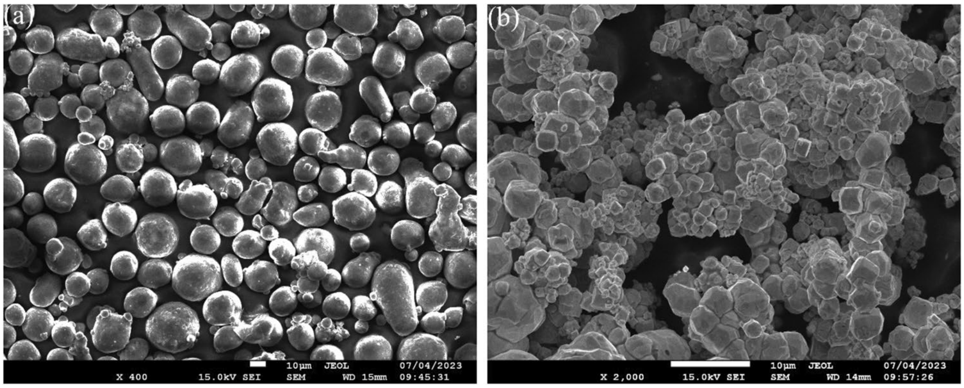

Fig. 2 Micrographs of SEM particles of pure aluminum and Wp: **a** Al powder, **b** Wp

Fig. 3 Experimental setups: **a** the pressure versus time plot during quasi-static compaction, **b** stress wave versus time curves during dynamic compaction by laser shock

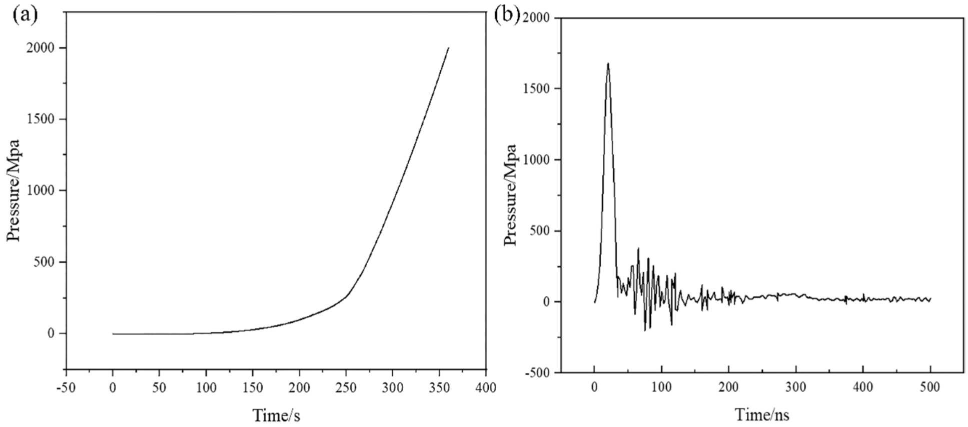

Table 2 Specific parameters of the molds used for the experiments

Parameter	Value
Energy per pulse (mJ)	600, 900, 1200, 1500, 1800
Spot diameter (mm)	Φ2.5
PMMA (mm)	Φ15 × 5
Micro die (mm)	Φ2.5 × 8
Black paint (μm)	50
Upper impactor (mm)	Φ2.498 ± 0.001 × 1.5
Lower impactor (mm)	Φ2.498 ± 0.001 × 7

recorded under a Vickers hardness tester (HXD-1000TMSC/LCD), setting the load parameters and the holding time to 50 gf and 15 s, respectively.

2.3 2D MPFEM modeling

As the dynamic response of the compressed billets could not be observed from a microscopic particle perspective during the experiments, we used 2D MPFEM to observe the compression process of the composite powders from a microscopic perspective. The discrete element method code, PFC 2D was used to generate the initial particle-filled structure of the composite powder (Wp/Al) with three Wp contents (5%, 10%, 15%), which were naturally stacked by gravity, before the multi-particle finite element. The position of the particles and the radius information were derived from PFC 2D and coupled to the FEM in 6.13 using a Python script. Figure 4 shows the specific model parameters imported into the FEM. Figure 4a shows the 2D MPFEM model imported into ABAQUS, where the Al particles and Wp are considered as circles in the simulation, with the Al particle size set to 20 μm and the Wp particle size set to 3 μm. Figure 4b displays the meshing of Al particles and Wp, where the Al particles and Wp are divided into quadrilateral structural elements, the number of quadrilateral structural elements of Al particles is 2541, and the number of quadrilateral structural elements of Wp is 243. Figure 4c displays the model of the randomly filled structure of the original particles of the compacted billets with different Wp contents.

2.3.1 Condition setting for the simulation

Given that the laser shock is an instantaneous process with a short time (< 1 μs), a dynamic explicit analysis was used in the simulation step, and the normal and tangential stresses are defined by the "penal" formulation of the Coulomb friction model and the "hard" contact model, respectively. The Cullen friction coefficient between the particles was set to 0.2 [22, 23]. The Al particles and Wp were set as elastic–plastic materials, the mold was set as a stiff body, and the three dimensions of freedom of mold were fixed during the analysis. Global remeshing [24] addresses the issues of over-distorted mesh and then remeshes the model to ensure that subsequent calculations can be performed successfully. Global remeshing is used on define each particle in the model to improve the computational accuracy of the simulation results and to obtain an accurate relative density of the compacts. A laser shock load was also used to the surface of the upper impactor based on the model established by Fabbro et al. [25] to convert the laser power density into peak pressure, the expression of which is shown below:

$$P_{max} = 0.01\left(\frac{\alpha}{2\alpha + 3}\right)^{\frac{1}{2}} \cdot Z^{\frac{1}{2}} \cdot {I_0}^{\frac{1}{2}} \quad (1)$$

where P_{max} (GPa) and α are the peak pressure during the laser shock and the ratio of thermal energy to the internal energy of the plasma, respectively, taking a value in the range of 0.1–0.2 in general. In this study, α takes the value of 0.1, I_0 is the power density of the laser, and Z is the acoustic impedance between the confined layer and the target, obtained by Eqs. (2) and (3), respectively:

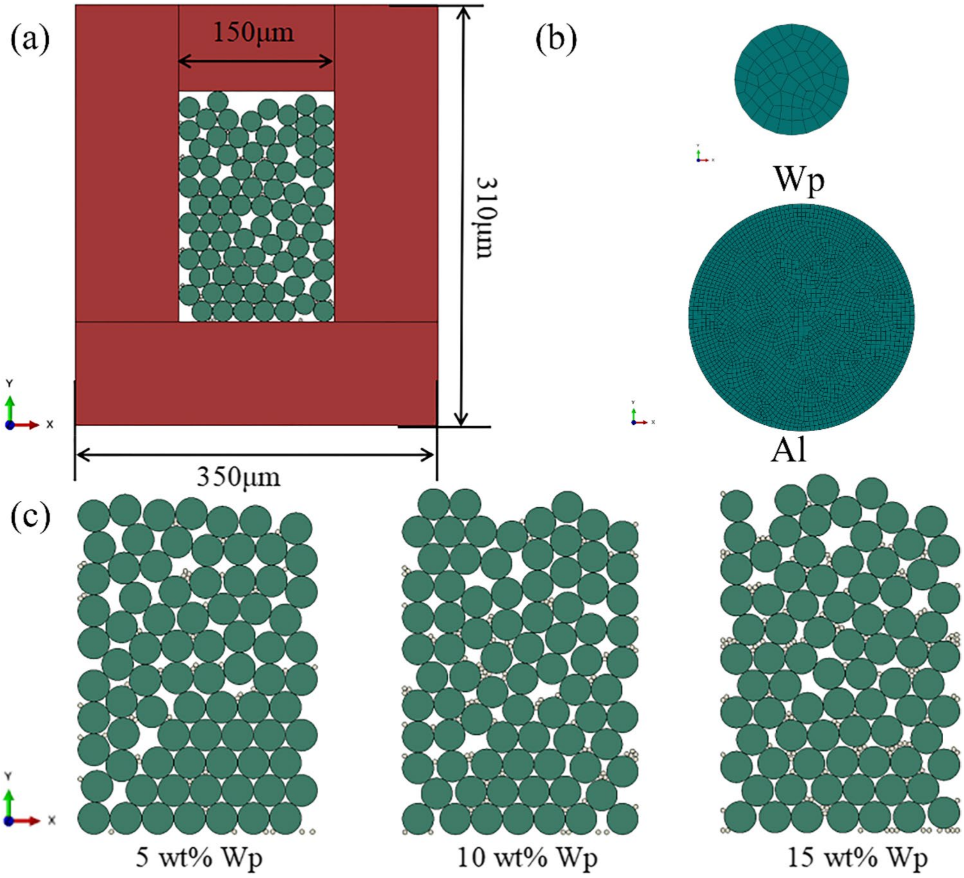

Fig. 4 T2D MPFEM model parameterization: **a** 2D model settings, **b** Al particle and Wp meshing, **c** model for the random packing structure of initial particles of pressed billets with different Wp contents

$$I_0 = \frac{4E}{\pi\tau D^2} \tag{2}$$

$$\frac{2}{Z} = \frac{1}{Z_1} + \frac{1}{Z_2} \tag{3}$$

where Z_1 (g/cm^2 · s) and Z_2 (g/cm^2 · s) are the constrained layer acoustic impedance and upper impactor acoustic impedance, respectively. In this study, $Z_1 = 0.32 \times 10^6$(g/cm^2 · s) and $Z_2 = 4.7 \times 10^6$(g/cm^2 · s). E (J), D (mm), and τ (ns) are the energy, spot diameter, and pulse width of the laser output, respectively. Given the presence of the confinement layer, the laser produces a pressure action time of approximately 2–3 times the laser pulse width; hence, in the simulation the laser shock in the load action time was set to 30 ns. The impact load curve with time is shown in Fig. 5, where the laser shock load peaks at approximately 10 ns. The analysis step is set to 1 μs in the simulation, thus ensuring the densification procedure of the Wp/Al composite powder.

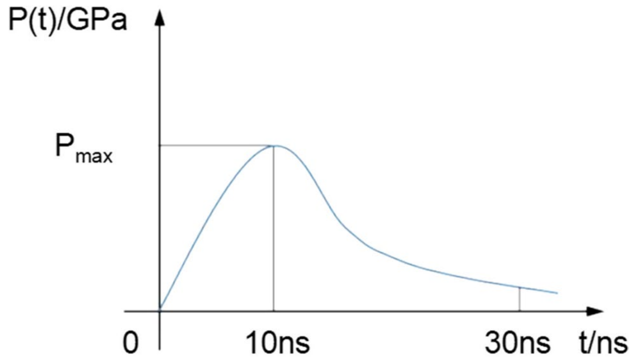

Fig. 5 Curve of impact loads over time

2.3.2 Intrinsic equations and selection of parameters

Given the extremely short laser high-speed shock time belonging to the high-strain rate dynamic compaction process, and involving the effects of temperature and procedure hardening, the Johnson–Cook model, which is widely used to characterize stress–strain behavior [26], was used in this study, and its formula is specified as follows:

$$\sigma = (A + B\varepsilon^n)(1 + Cln\frac{\dot{\varepsilon}}{\dot{\varepsilon}_0})\left[1 - (\frac{T - T_r}{T_m - T_r})^m\right] \tag{4}$$

where A, B, n, and m are the intrinsic parameters of the material; ε is the equivalent plastic strain, $\dot{\varepsilon}$ is the strain rate,$\dot{\varepsilon}_0$ is the reference strain rate, and T, T_r, and T_m are the current, ambient, and initial melting temperatures, respectively. The intrinsic parameters of Al and Wp are shown in Table 3.

3 Results and discussion

3.1 Variation in relative density for different pressing press pressures

Figure 6 shows an experimental comparison of the compacts obtained by laser shock dynamic compaction and quasi-static compaction. Figure 6a shows the billets of three Wp content (5%, 10%, 15%) composite powders obtained by laser shock dynamic compaction and quasi-static compaction under the same pressure; the figure reveals that the billets obtained under both modes of action are cylindrical blocks with no evident defects. Figure 6b shows the trend of the relative density. As shown in Fig. 6b, the relative density of the compacted billets showed a decreasing trend with increasing of Wp content, whereas the pressure was kept constant, and the relative density reached a maximum at a Wp content of 5%. When the Wp content was the same, the relative densities of the billets obtained by laser shock dynamic compaction were higher than those obtained under quasi-static conditions, and the relative densities increased by 0.69%, 1.31%, and 2.9% as the Wp content increased.

To investigate further the trend of relative density variation of composite powders with different Wp contents under different loading pressures for laser shock dynamic compaction versus quasi-static compaction, Fig. 7 shows the trend of the relative density of the compacted billet with loading pressure for both laser shock dynamic compaction and quasi-static compaction. As shown in Fig. 7a, with the increase in laser shock pressure, the relative density of the billet gradually increases, and at the lower laser shock pressure, the relative density of the billet increases faster, which is mainly attributed to the large pores between particles in the early stage; moreover, the increase in the density mainly relies on the elimination of the pores. Later, with the growth of the laser shock pressure, the increase in the density is mainly due to the plastic deformation of Al particles. Figures 7b–d show that when the pressing pressure is less than 2300 MPa, the relative density of the compacts obtained by quasi-static compaction is higher than that obtained by laser shock dynamic compaction, which is mainly because under quasi-static compaction the particles have enough time to rearrange and rotate when the pressure is small, which in turn leads to faster elimination of the pores between the particles. When the compaction pressure is greater than 2300 MPa, dynamic compaction with laser shock gradually increases the relative density of the billet over that of quasi-static compaction, because quasi-static compaction of hard reinforced particles Wp rearranges and aggregates, preventing further plastic deformation of the aluminum particles, resulting in a reduction in densities. By contrast, laser shock dynamic compaction enables the powder to be impacted at high speed in a short period time and the particles are rearranged briefly and subjected to a large plastic deformation.

Table 3 Intrinsic parameter settings for Al particles and Wp [20]

Property	Al	Wp
Density (kg ·m^{-3})	2.78×10^3	19.35×10^3
Elastic modulus (MPa)	69,000	133,000
Poisson’s ratio	0.27	0.22
A (MPa)	148.361	1510
B (MPa)	345.513	177
n	0.183	0.12
m	0.859	1
T_m (°C)	660	3660
T_r (°C)	25	25

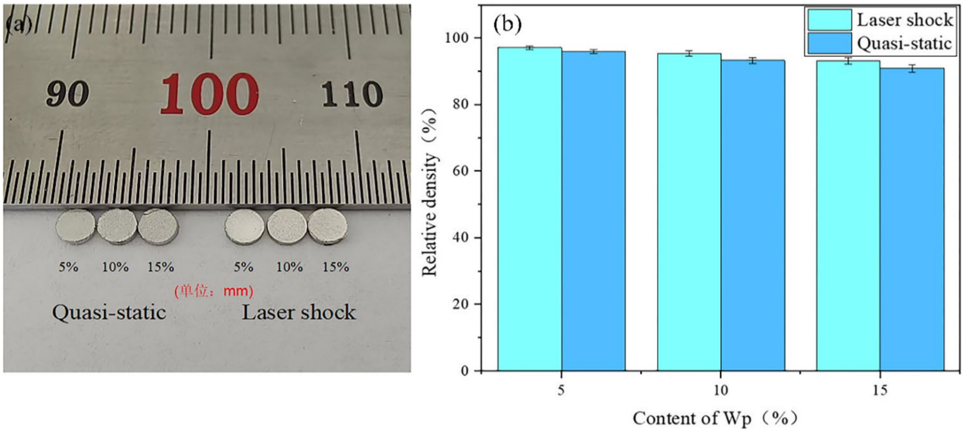

Fig. 6 Compacted billets of three Wp-content composite powders under laser shock and quasi-static: **a** physical diagram of compacted volume, **b** relative density variation of the compact

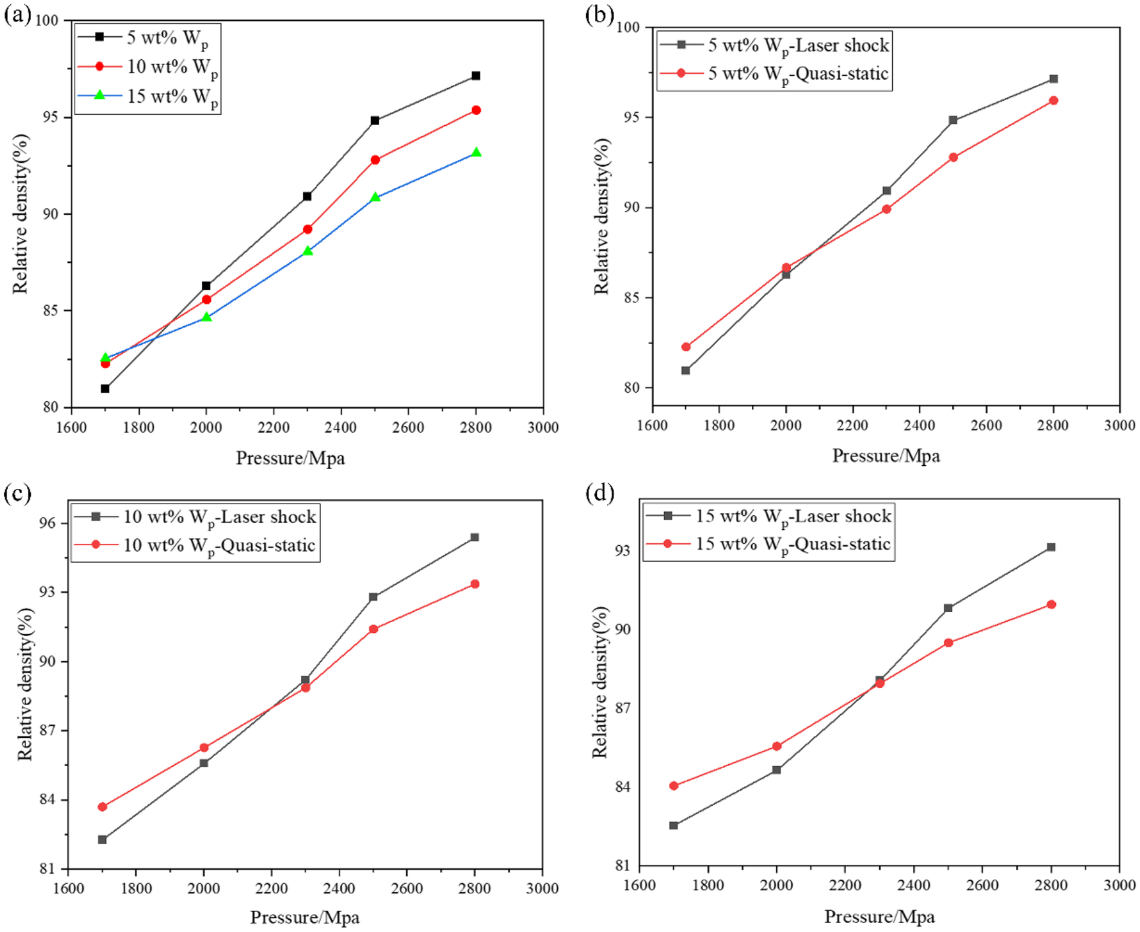

Fig. 7 Trends in the relative density of laser shock dynamic compaction and quasi-static compaction of composite powders with different Wp contents at different loading pressures: **a** links between laser shock pressure and the relative density of pressed billets, **b**–**d** trends in the relative density of composite powders under dynamic compaction with laser shock and quasi-static compaction

3.2 Surface microstructure analysis of pressed billets

The homogeneous distribution of hard particles is crucial to the isotropy and stress distribution of the composite. To visualize the distribution of hard particles Wp, Fig. 8 shows the surface microstructure of three Wp-content composite powder compacts under dynamic compaction with laser shock and quasi-static compaction at the same pressure. Figures 8a–c show the surface microstructure of the compacted billets under dynamic compaction by laser shock and Figs. 8b–d show the surface microstructure of the compacted billets under quasi-static compaction. As the Wp content increases, corresponding voids appear on the surface of the billet because the hard particle Wp hinders the plastic deformation of the Al particles, leading to a considerable increase in the number of pores and consequently a decrease in the densities. When the Wp content is the same, Wp aggregation and thus Wp clustering can be found in the compacted billet under quasi-static compaction [27]. However, almost no aggregation occurs under dynamic laser shock compaction. The reason is that during quasi-static compaction, the compaction pressure is a process that gradually increases with time, giving the Wp particles sufficient time to slide, rearrange, and aggregate together; by contrast, laser shock is an instantaneous process with a small rearrangement of the Wp particles, resulting in large plastic deformation of the Al particles within a short period and uniform distribution of the hard Wp particles around the Al matrix, resulting in less aggregation. Figure 8 reveals that the boundaries of the Al particles in the compaction blanks under laser shock dynamic compaction are all bound together because the duration of laser shock dynamic compaction is considerably short, on the order of 1 μs, resulting in densification at very high strain rates, whereas the energy transferred during laser shock dynamic compaction causes the Al particles to be subjected to huge strains and collisions and friction in a

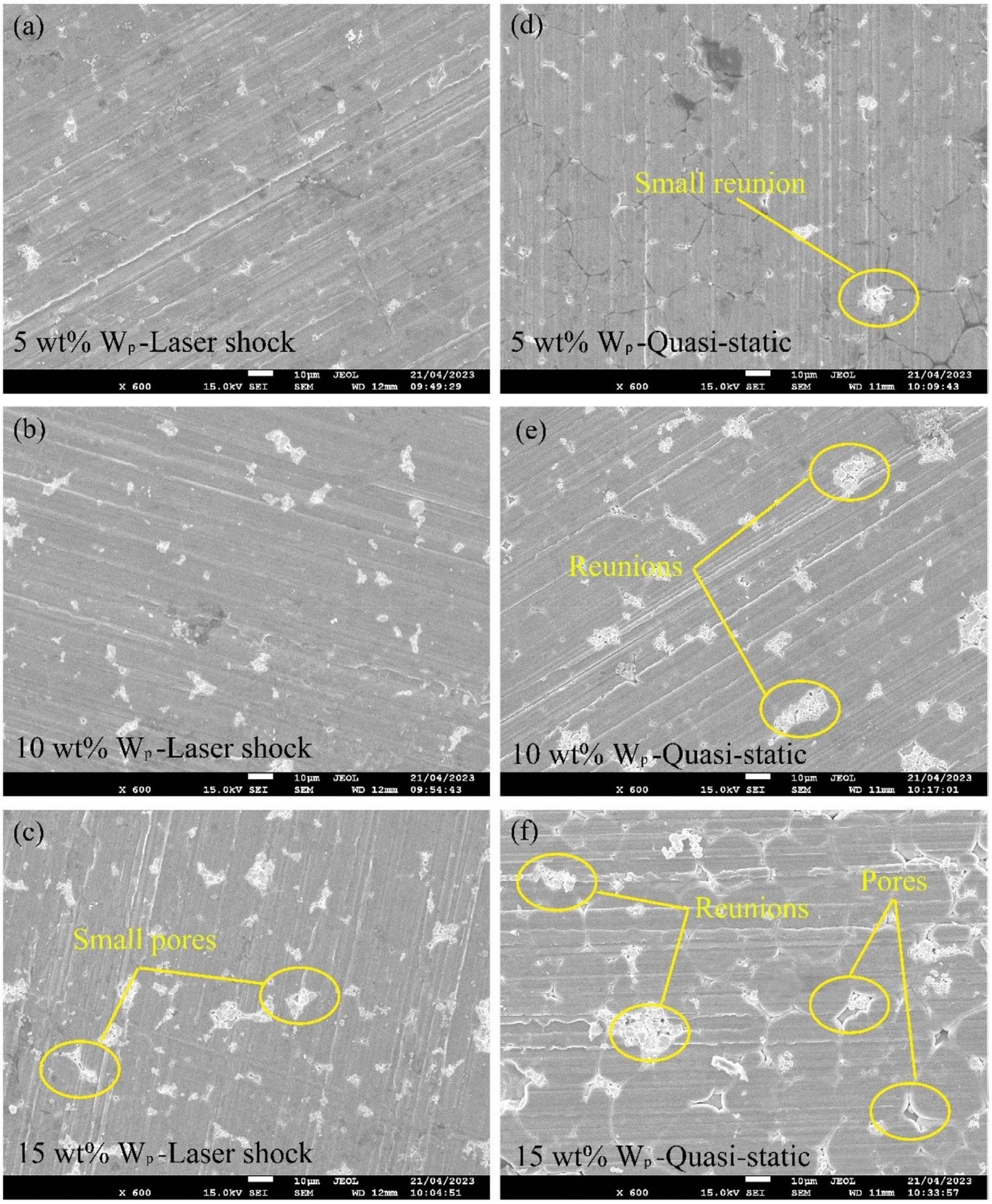

Fig. 8 Surface microstructure of pressed billets: **a**–**c** surface microstructure of the compacted billet under dynamic compaction by laser shock, **d**–**f** surface microstructure of a pressed billet under quasi-static compaction

short period. The heat generated during this process is adiabatic, i.e., the energy converted to heat does not have sufficient time to dissipate, and therefore the heat generated causes a local temperature rise on the surface of the particles leading to a softening of the surface, which is easier to deform and allows for the possibility of interfacial melting [28]. This result is consistent with the analysis by Yi et al. [11] and Nieh et al. [29] of the possibility that dynamic impacts on powders can cause a large amount of heat to accumulate within the powder, resulting in a local temperature increase that allows the surface of the particles to soften and melt.

3.3 Analysis of demolding pressure

The release pressure during demolding (the pressure required to release the billet from the mold after the pressing pressure has been unloaded) is a key factor in the integrity of press billets. To measure the demolding pressure under dynamic and quasi-static compaction with laser shock,

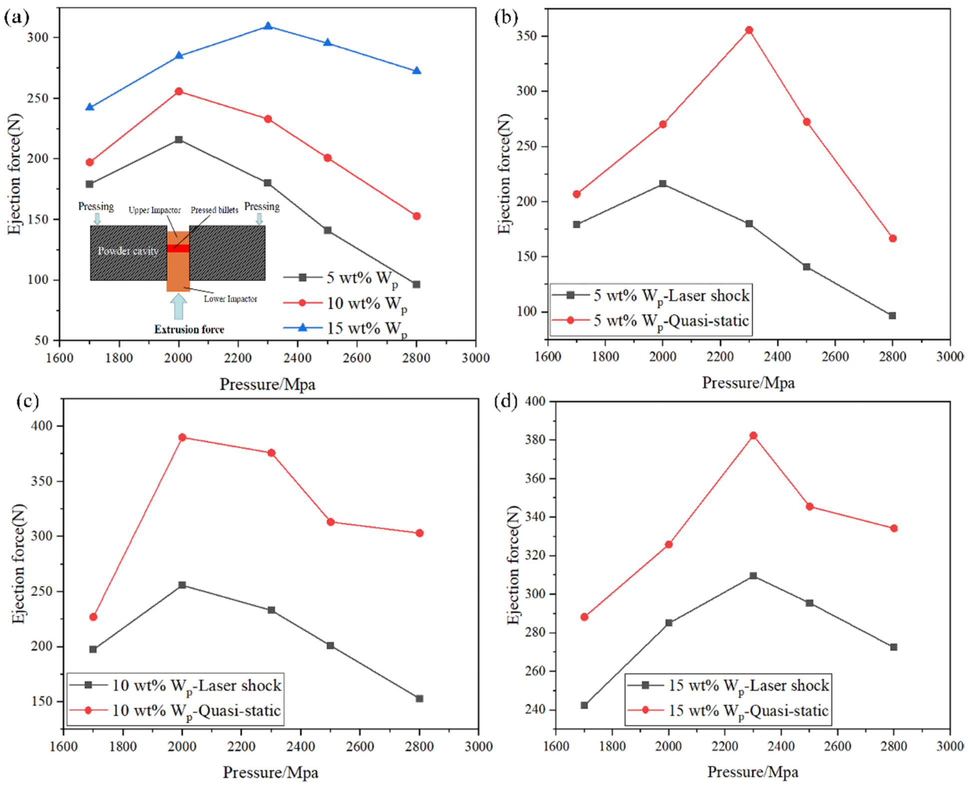

Fig. 9 Demolding pressures for press blanks obtained at high versus low strain rates: **a** relationship between molding pressures and laser shock pressures, **b**–**d** comparison of demolding pressures for dynamic compaction with laser impact at high strain rates and quasi-static compaction of press blanks at low strain rates

the finished composite powder billets were slowly pressed under a CNC press and the peak pressure during demolding was recorded, with each set of data averaged three times. Figure 9 displays the change in the demolding pressure at different pressures under dynamic and quasi-static compaction with laser shock. Figure 9a displays the change curve of the demolding pressure under different laser shock pressures and the demonstration of the demolding principle. As shown in the figure, as the laser impact pressure increases, the demolding pressure shows a trend of rising and then falling, because when the pressing pressure is small, the joint strength between the particles is weak, resulting in a small demolding pressure, and when the laser impact pressure increases further, the demolding pressure shows a decreasing trend, which is mainly attributed to the composite powder in the laser high-strain rate high-speed impact, the upper layer of particles plastic deformation at the same time the upper layer of particles were given a very high acceleration rushed to the lower layer of particles, due to inertial effect of the lower layer of particles by serious friction and collision at the same time serious plastic deformation, at this time the formation of high-strength mechanical connection between the powder block, the powder within the plastic deformation of the dominant energy, and a very small part of the energy exists in the elastic energy, which leads to the reduction of the radial rebound of the billet, so the demolding pressure will show a decreasing trend. Figure 9a shows that the release pressure gradually increases as the Wp content increases, with the increase of Wp content, due to the hard particles Wp will hinder the plastic deformation of aluminum particles, from Fig. 8, it can be found that with the increase of Wp content of the billet will eventually appear pores, for the release of the elastic stress wave in the powder body to provide a space to change the contact state of the particles will lead to the bonding of the particles will be weakened, the radial rebound will be increased, and therefore in the process of demolding the demolding pressure will increase. Figures 9b–d show the difference in demolding pressure between laser shock dynamic compaction and quasi-static compaction for the three Wp contents of the composite powder billets. The demolding pressure of the billets obtained by laser shock dynamic compaction is smaller than that of the billets obtained by quasi-static compaction, this is mainly due to the fact that the compaction obtained by laser shock dynamic compaction results in a high strength bond between the particles, which has a positive effect on the reduction of the radial springback [9], which in turn leads to a significant reduction of the demolding pressure, and with increasing of Wp content, the demolding pressure decreases by 1.56, 1.55, and 1.19 times on average; similar findings were obtained by Yi et al. [11]. Figure 10 shows the radial springback comparison between laser shock and quasi-static compaction of composite powders with different Wp contents under the same pressure, and it can be found that the radial springback of the compression billet under laser shock compaction is smaller, mainly because the laser shock

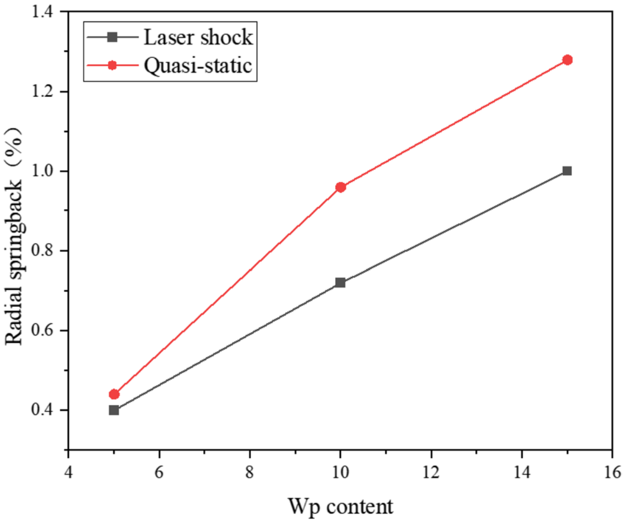

Fig. 10 Comparison of radial springback of composite powders with different Wp content under laser shock and quasi-static compaction

process is adiabatic, and most of the heat generated does not have time to dissipate, and the compression billet produces smaller springback due to the lower yield strength, and the compression billet shrinks when it is cooled down [28].

3.4 Microscopic microhardness analysis

The uniformity of the microhardness distribution of a pressed billet is closely related to its mechanical characteristics. To investigate the microhardness spread inside the billet and the effect of Wp particle content on the hardness of the billet, the billet was previously set in epoxy resin and fixed and then sandpapered to the maximum diameter of the billet and polished. Finally, the hardness spread was measured in different areas of the billet cross-section. Figure 11 shows the microhardness distribution of the billet cross-section obtained by laser shock at high strain rates and quasi-static compaction at low strain rates, where the upper, middle, and lower parts of the cross-section are selected in the radial direction and nine points are selected for microhardness measurement in each of these areas. Figures 11a–c show the microscopic microhardness distribution under dynamic compaction with laser shock and Figs. 11d–f show the microscopic microhardness distribution under quasi-static compaction. The average microhardness of the billets increases with increasing Wp particle content, which is mainly attributed to the addition of hard reinforced Wp particles, but the average microhardness distribution of the billets obtained by quasi-static compaction at low strain rates has a wide range between different regions due to the inhomogeneous distribution of the hardness distribution of the billets caused by the agglomeration of the reinforced Wp particles. During the laser shock process, as the powder is dynamically impacted at a high strain rate, violent deformation occurs between the particles, resulting in some process hardening of the powder. Given the inertial effect, almost no rearrangement of the hard particles Wp occurs, resulting in a more even hardness dispersion between the various areas of the pressed billet, while the hardness increases by 9.5%, 13.5%, and 11.8% compared with the pressed billet obtained quasi-statically.

3.5 Analysis of 2D MPFEM results

3.5.1 Analysis of relative densities in simulation

To investigate the associations between different laser shock pressures and the relative density of the compacts, five laser shock pressures (600, 900, 1200, 1500, 1800 mJ) were selected for laser dynamic compaction simulations on three Wp (5%, 10%, 15%) composite powders. Figure 12 shows the variation in the relative density of the billets with the laser impact pressure. Figure 12a shows that the relative density of the billet gradually increases as the laser shock pressure increases, and reaches a maximum of 97.62% at a Wp content of 5%. Figures 12b–d show the comparison between the laser shock dynamic compaction experiment and the simulation. It can be found that the relative density variation curves in the experiment and the simulation are highly similar, thus verifying the feasibility and accuracy of the 2D MPFEM.

3.5.2 Velocity analysis in the press billet

During dynamic compaction by laser high-speed shocks, the stress wave propagates from the upper impactor to the lower impactor in the form of an approximately one-dimensional plane wave, so that the problem of impact compression of granular materials can be reduced to a one-dimensional problem for analysis. A one-dimensional speed field distribution is imported to quantify the propagation characteristics of surface evidence shock waves. The speed data of each node at different moments in the Lagrangian coordinate system can be directly obtained from the simulation analysis results; thus, a path (Figs. 13a–c) at each of the three Wp contents (5%, 10%, 15%) is chosen and the velocity information of each node on the path is extracted, as shown in Figs. 13d–f. When $t = 50$ ns, the laser shock produces a huge impact force on the upper impactor and gives the upper layer of particles a considerably high acceleration, the upper layer of particles obtains a certain speed and accompanied by plastic deformation rushed to the lower level of particles, the upper level of particles in the majority of the dynamic into the kinetic energy of the lower level of particles, a small part of the energy into strain energy, friction energy; thus, the upper level of particles in the laser impact of high-speed

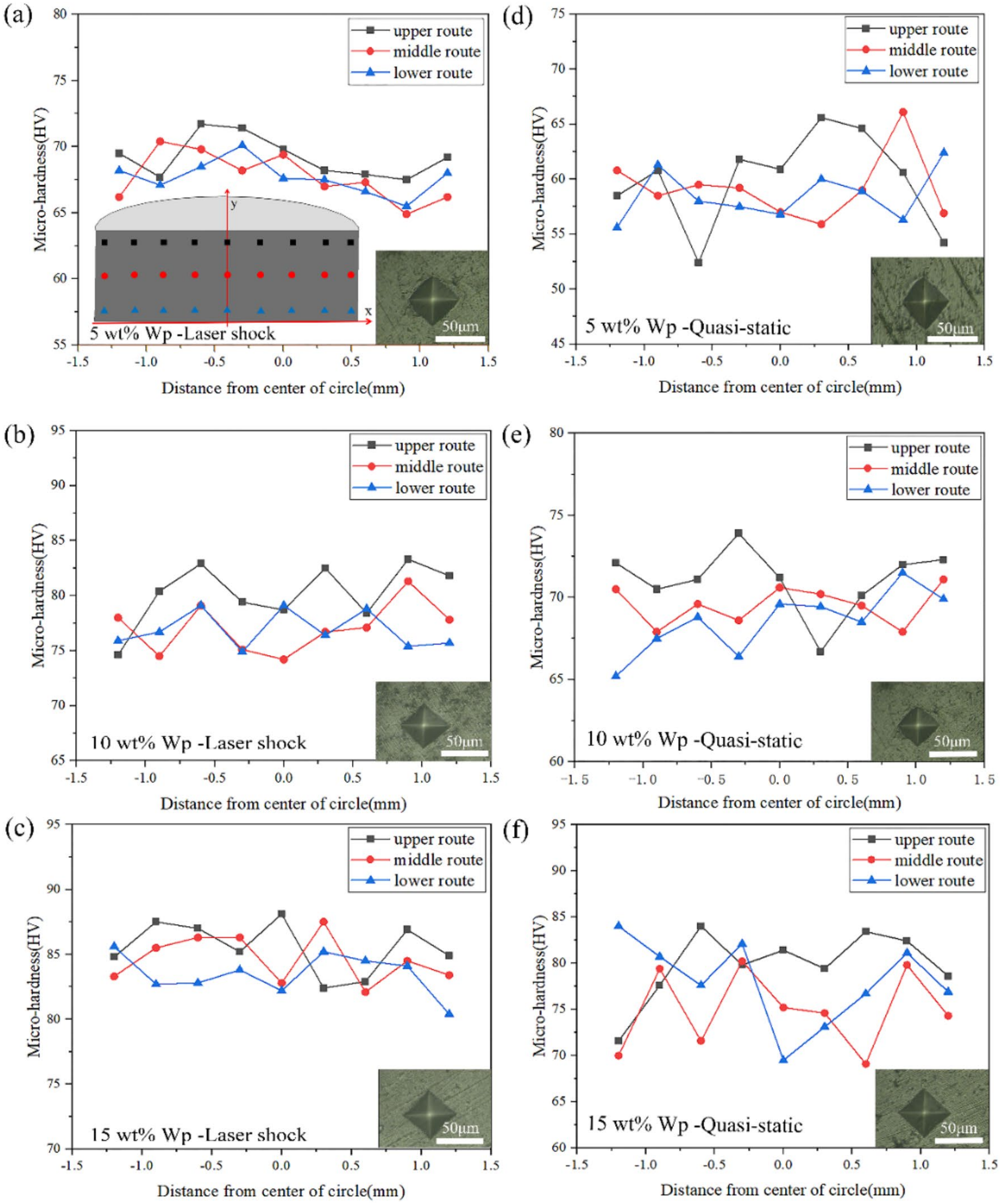

Fig. 11 Variation in hardness of nodes on different areas of a composite powder (Wp/Al) press billet: **a**–**c** trends in microhardness of compacted billets obtained under dynamic compaction with high-strain rate laser shock, **d**–**f** trends in microhardness of compacted billets obtained by quasi-static compaction at low strain rates

deformation first. When $t = 250$ ns, the shock wave propagates to the bottom of the billet, and the particle speed gradually decreases under the obstruction of the lower impactor. The velocities show a gradient of decreasing velocity at different moments in the process of laser impact, with a larger decrease in velocity at each moment as the Wp content increases, mainly because the overfilling of Wp can impede the propagation of shock waves between Al particles. In the study, the higher the laser shock pressure was, the greater the wave speed, which is in line with the Hugoniot associations. The collision welding of metallic materials has a minimum velocity V_{pmin} within a short time, and the minimum

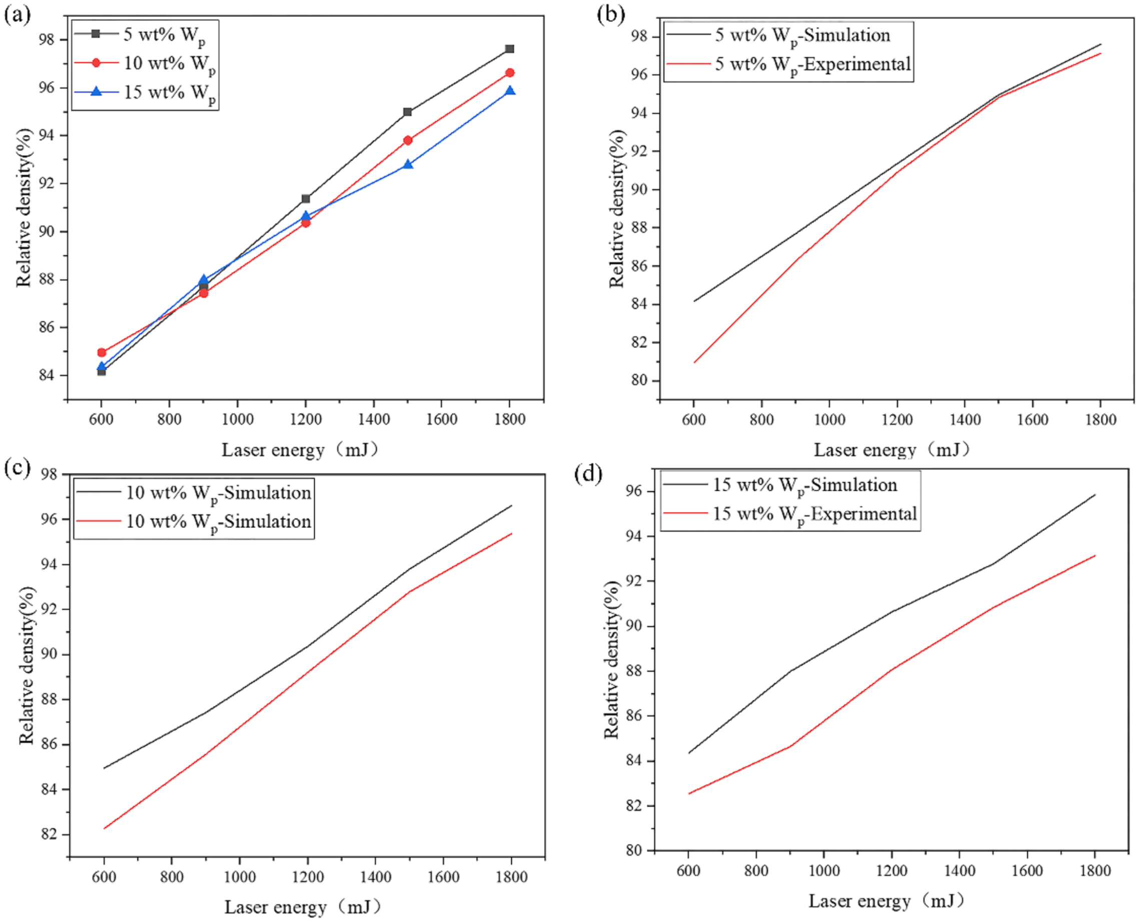

Fig. 12 Variation curves of relative densities of pressed billets in simulations: **a** relationship between relative densities in simulations, **b**–**d** comparison of simulated and experimental relative density changes at different laser energies

collision velocity V_{pmin} between Al materials is 189 m/s [30]. The graph shows that the particles velocity in the composite powder (Wp/Al) is greater than 189 m/s before $t = 100$ ns; thus, the cold welding between the particles can basically be accomplished under high-speed laser shock.

3.5.3 Densification procedure by laser shock dynamic compaction

To visualize the densification process during dynamic compaction by laser shock, Fig. 14 shows the flow of particles inside the composite powder during compaction, where the directional synthesis vector of particle movement is represented by an arrow. When $t = 75$ ns, there is a large pore space appears between the particles, and the upper impactor is in high-speed contact with the upper particles. Given that the inertial effect of the upper particles first causes larger plastic deformation, the upper particles undergo larger displacement, the particles mainly flow to the pore space and are larger, and the bottom particles do not move. When $t = 200$ ns, when the upper level of particles undergoes larger plastic deformation, the upper level of the region reaches densification, and the relative density of the pressed billet increases faster; at this time, the direction of the particle flow vector is down. At $t = 300$ ns, full densification is reached between the particles. Given the obstruction of the lower impactor, the bottom particles flow into the pores between the particles and the inner wall of the powder chamber, and the lower part of the area reaches densification. In general, during laser shock compaction, the particles experience plastic deformation and densification in a considerably short time from an initial velocity of zero due to the extremely short duration of the laser shock process, which in turn generates extremely high acceleration of the particles, resulting in strain inertia and enhances the shape-ability of the composite powder. The Al particles all experience large plastic deformation; the hard particles Wp are uniformly distributed around the Al particles. When the Wp content increases, as the hard particle Wp is much harder than the Al particles, Wp does not deform during the simulation and prevents the plastic deformation of the Al particles; thus, certain voids appear between the particles in the press billet, resulting in

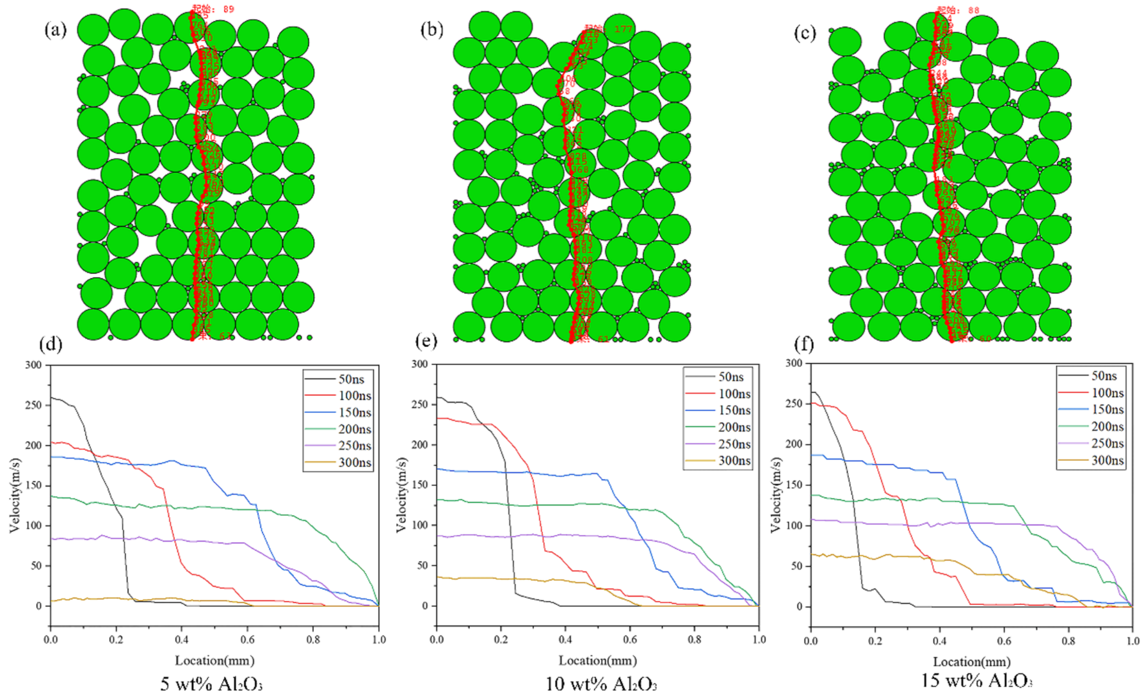

Fig. 13 Velocity information of path nodes in compression billets with different Wp contents. **a–c** path building for the model, **d–f** variation of velocity with time in the path phase of the pressed billet model for different Wp contents

a further decrease in the relative density of the compacted billet, and the inter-particle pores are mainly formed by the pores between Al–Al and Wp–Wp, which is consistent with Fig. 8c. The analysis of the surface structure of the press billets in the experiment is consistent.

3.5.4 Adiabatic temperature rise phenomena

In the process of dynamic compaction by laser shock due to collision, friction, and plastic deformation of the particles in a short period, a large amount of heat accumulates inside the particles and cannot be diffused in a short period, resulting in a local temperature rise at the edges of the particles, a phenomenon known as adiabatic temperature rise. Figure 15 shows the temperature rise clouds for the final simulated press billets for three Wp contents (5%, 10%, 15%), with the initial temperature set at 20 °C in the simulation. The kinetic energy obtained by the upper punch is gradually transformed into the kinetic energy of the upper layer of particles in contact with the upper punch (Fig. 15a), which is accompanied by plastic deformation. After the upper impactor is in stable contact with the upper layer of particles, the pressed billet starts to enter the densification stage, the plastic deformation energy E_p of the particles gradually increases, the friction energy E_F is accompanied by a slight increase, and the plastic deformation energy E_p dominates at this time. Moreover, the heat between the particles mainly comes from the plastic deformation of the particles and friction. Figures 15b–d show that the inter-particle heat is mainly concentrated in the particle-to-particle contact area, and the local temperature is generally greater in the contact area with the upper impactor than in the middle and bottom areas.

To reflect the local temperature trend with time during the laser shock process, the variation pattern of the particle node temperature in the press billet was selected, as shown in Fig. 16. As shown in Fig. 16a, the edge nodes ABCD and the internal nodes A′B′C′D′ of the upper and middle layers of particles were selected, and the temperature of the edge nodes of the upper layer of particles is found to be basically close to the melting point of Al particles at 660 °C, whereas the temperature of the edge of particles in the middle region is only approximately 100 °C. The temperature at the edge nodes of the particles near the walls of the powder cavity is greater than the temperature at the edge nodes of the particles in the middle layer, mainly due to the additional heat generated by the friction close to the walls of the powder cavity. As shown in Fig. 16b, the internal node temperature of the particles is lower than the node temperature at the edge of the particles, and the temperature at the middle node of the upper layer of particles is higher than the temperature at the center node of the middle layer of particles; thus, during the laser high-speed shock process, the higher local temperature occurs mainly at the contact with the upper impactor and the temperature at the edge of the particles is much higher than the temperature inside the particles.

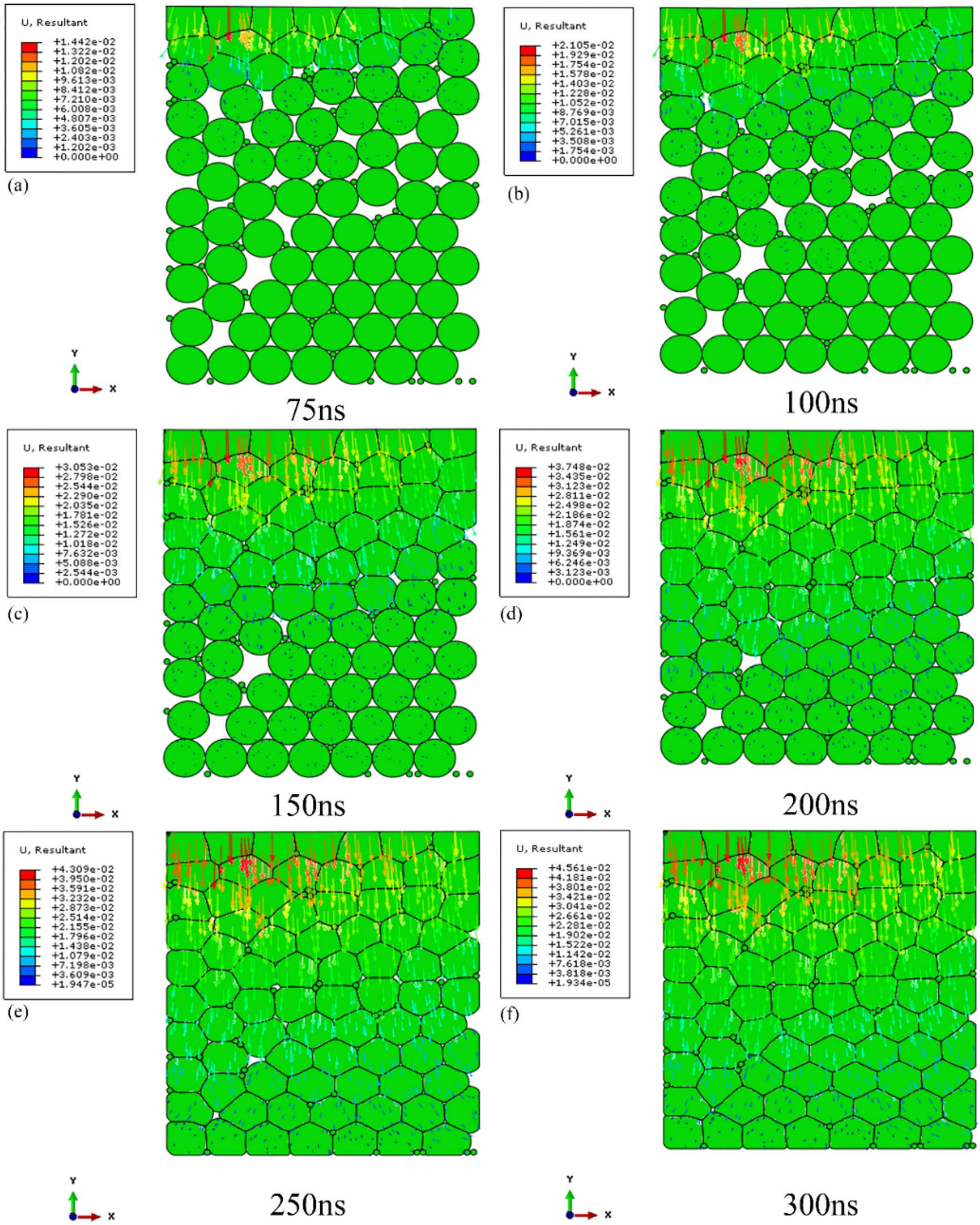

Fig. 14 **A–f** Particle movement in the composite powders with the compaction process

4 Conclusion

The effects of pressing pressure and Wp content on the relative density, surface microstructure, inter-particle connection mechanism, demolding pressure, radial rebound, and microhardness distribution of Al-based composite powder (Wp/Al) compacts were analyzed by conducting dynamic compaction experiments with high-strain rate laser shock and quasi-static compaction with low strain rate. The shock wave propagation, densification, and adiabatic temperature rise in the pressed billet at high strain rates due to laser shock were analyzed in combination with 2D MPFEM. The following conclusions were obtained:

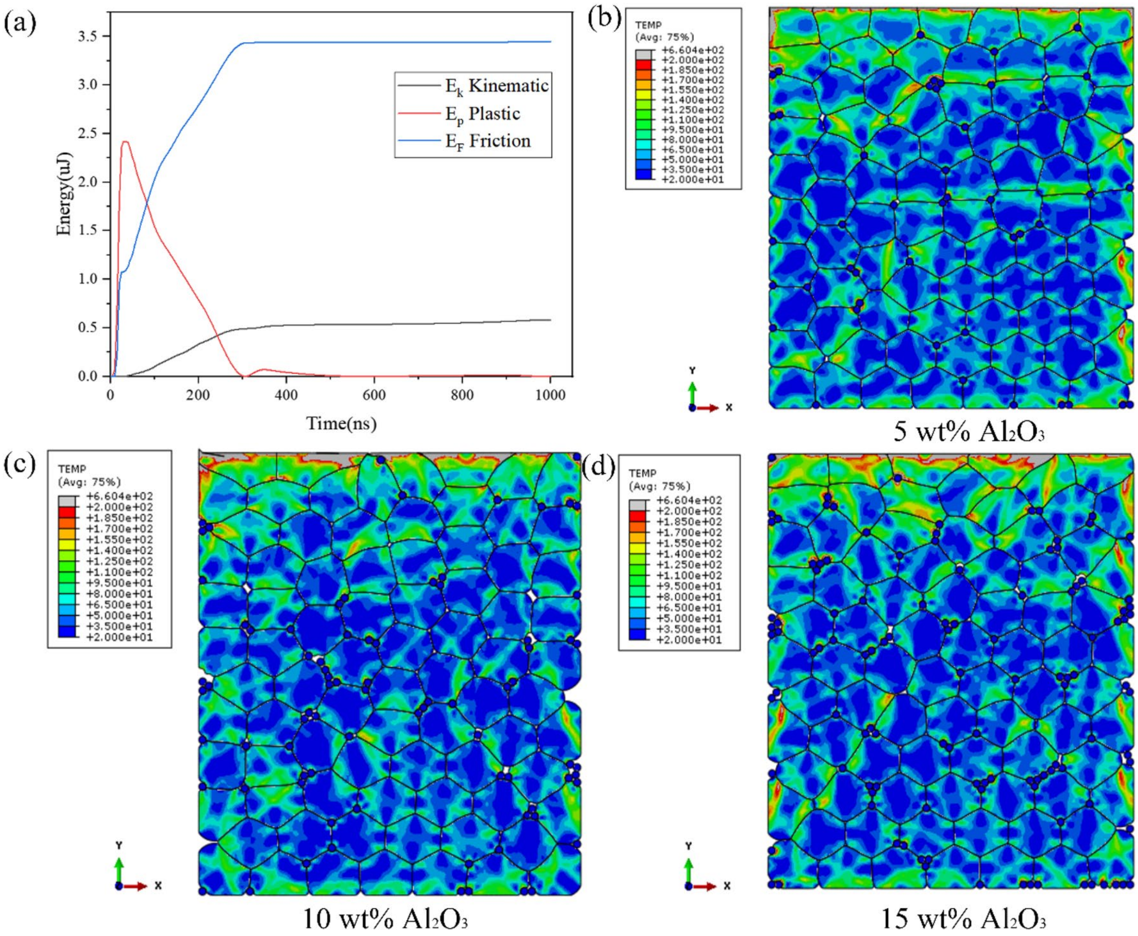

Fig. 15 Temperature variation results for models with three Wp contents (5%, 10%, 15%): **a** trend of the overall energy of the press billet with time, **b**–**d** temperature rise clouds of the final simulated press billet for the three Wp contents

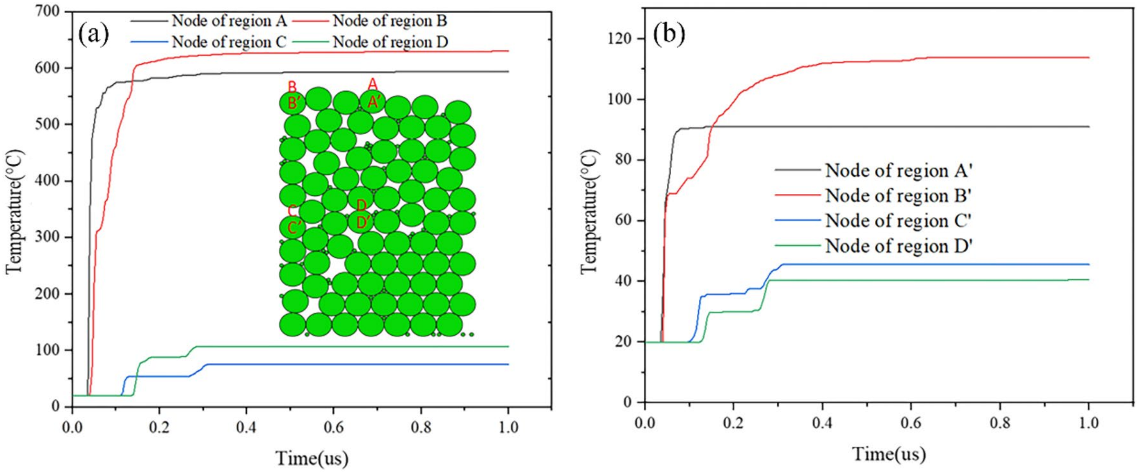

Fig. 16 Temperature trends at the edge nodes of the particles in different regions as well as at the internal nodes: **a** temperature variation at the edge nodes of the particles in different regions, **b** temperature variation at the internal nodes of the particles in different regions

1) With the growth of pressing pressure, the relative density of the composite powder billets shows an increasing trend with the pressing pressure. As the Wp content increases, the final relative density of the pressed billets gradually decreases and reaches a maximum at Wp contents of 5%, but the relative density of the billets obtained by high-strain-rate laser shock dynamic compaction increases by up to 2.9% in comparison with low-strain-rate quasi-static compaction.
2) A comparison of the experimental results shows that the billets obtained under dynamic compaction with high-strain rate laser shock have 1.56 times lower molding pressure and 13.5% higher hardness than those obtained under quasi-static compaction with low strain rate.
3) 2D MPFEM can better observe the dynamic mechanical response in the dynamic compaction process of laser impact from the perspective of particles and can intuitively observe the inertia effect, shock wave propagation effect, and adiabatic effect in the composite powder. In the high-speed laser shock process, the particles produce serious plastic deformation due to the inertia effect, and the inter-particle can better achieve the metal connection; the speed of the inter-particle in the powder basically reaches the minimum collision speed of welding, which is conducive to the inter-particle can achieve better bonding; the temperature at the edge of the particle is basically greater than that inside the particle, and the temperature near the upper impactor is higher.

Author contribution TW: investigation, writing—original draft preparation; MC: validation, methodology; ZZ: conceptualization; HL: writing—review and editing, supervision; YM: formal analysis; WS: resources; XW: validation.

Funding The work reported in this paper was supported by the National Natural Science Foundation of China (No. 51675243 and No. 52075226).

Declarations

Competing interests The authors declare no competing interests.

References

1. Yan Z, Chen F, Cai Y (2011) High-velocity compaction of titanium powder and process characterization. Powder Technol 208:596–599. https://doi.org/10.1016/j.powtec.2010.12.026
2. Eriksson M, Andersson M, Adolfsson E, Carlström E (2013) Titanium–hydroxyapatite composite biomaterial for dental implants. Powder Metall 49:70–77. https://doi.org/10.1179/174329006x94591
3. Yim D, Kim W, Praveen S, Jang MJ, Bae JW, Moon J, Kim E, Hong SJ, Kim HS (2017) Shock wave compaction and sintering of mechanically alloyed CoCrFeMnNi high-entropy alloy powders. Mater Sci Eng A 708:291–300. https://doi.org/10.1016/j.msea.2017.09.132
4. Li H, Yin HQ, Khan DF, Cao HQ, Abideen Z, Qu XH (2014) High velocity compaction of 09Al2O3/Cu composite powder. Mater Des 57:546–550. https://doi.org/10.1016/j.matdes.2013.12.059
5. Zhang H, Zhang L, Dong G, Liu Z, Qin M, Qu X (2016) Effects of warm die on high velocity compaction behaviour and mechanical properties of iron based PM alloy. Powder Metall 59:100–106. https://doi.org/10.1179/1743290115y.0000000019
6. Khan DF, Yin H, Li H, Qu X, Khan M, Ali S, Iqbal MZ (2013) Compaction of Ti–6Al–4V powder using high velocity compaction technique. Mater Des 50:479–483. https://doi.org/10.1016/j.matdes.2013.03.003
7. Yan ZQ, Chen F, Cai YX, Yin J (2013) Influence of particle size on property of Ti–6Al–4V alloy prepared by high-velocity compaction. T Nonferr Metal Soc 23:361–365. https://doi.org/10.1016/s1003-6326(13)62470-x
8. Zhou J, Zhu CY, Zhang W, Ai WT, Zhang XJ, Liu K (2020) Experimental and 3D MPFEM simulation study on the green density of Ti–6Al–4V powder compact during uniaxial high velocity compaction. J Alloys Compd 817:153–226. https://doi.org/10.1016/j.jallcom.2019.153226
9. Cui JJ, Huang XS, Dong DY, Li GY (2020) Effect of discharge energy of magnetic pulse compaction on the powder compaction characteristics and spring back behavior of copper compacts. Met Mater Int 27:3385–3397. https://doi.org/10.1007/s12540-020-00698-6
10. Bayle JP, Jorion F (2012) High velocity compaction: comparison with conventional compaction for new press development in hot cell pellet manufacturing. Procedia Chemistry 7:431–443. https://doi.org/10.1016/j.proche.2012.10.067
11. Yi M-J, Yin H-Q, Wang J-Z, Yuan X-J, Qu X-H (2009) Comparative research on high-velocity compaction and conventional rigid die compaction. Front Mater Sci China 33:447–451. https://doi.org/10.1007/s11706-009-0057-5
12. Dong DY, Huang XS, Li GY, Cui JJ (2020) Study on mechanical characteristics, microstructure and equation of copper powder compaction based on electromagnetic compaction. Mater. Chem. Phys. 253. https://doi.org/10.1016/j.matchemphys.2020.123449
13. Dong DY, Huang XS, Cui JJ, Li GY, Jiang H (2020) Effect of aspect ratio on the compaction characteristics and micromorphology of copper powders by magnetic pulse compaction. Powder Technol 31:4354–4364. https://doi.org/10.1016/j.apt.2020.09.010
14. Atrian A, Majzoobi GH, Enayati MH, Bakhtiari H (2014) Mechanical and microstructural characterization of Al7075/SiC nanocomposites fabricated by dynamic compaction. Int J Miner Metall Mater 21:295–303. https://doi.org/10.1007/s12613-014-0908-7
15. Sharma AD, Sharma AK, Thakur N (2012) Crystallographic and morphological characteristics of explosively compacted copper under various detonation velocities. Philos Mag 92:2108–2116. https://doi.org/10.1080/14786435.2012.669057
16. Wang X, Hou X, Zhang D, Gong Q, Ma Y, Shen Z, Liu H (2022) Research on warm laser shock sheet micro-forging. J Manuf Processes 84:1162–1183. https://doi.org/10.1016/j.jmapro.2022.10.076
17. Hou X, Ma Y, Wang X, Shen W, Cui M, Liu H (2023) Size effect of laser shock sheet bulk microforging. Int J Adv Manuf Technol 128:2719–2737. https://doi.org/10.1007/s00170-023-12094-6
18. Yan Z, Ma Y, Liu H, Wang X (2023) Investigation on formability and mechanism in laser shock hydraulic warm free-bulging of AZ31B magnesium alloy foils. Int J Adv Manuf Technol 126:505–517. https://doi.org/10.1007/s00170-023-11143-4
19. Zheng C, Zhang X, Liu Z, Ji Z, Yu X, Song L (2018) Investigation on initial grain size and laser power density effects in laser shock bulging of copper foil. Int J Adv Manuf Technol 96:1483–1496. https://doi.org/10.1007/s00170-018-1722-6

20. Ni P, Liu HX, Dong Z, Ma YJ, Wang X (2022) Laser shock dynamic compaction of aluminum powder. J Manuf Processes 77:694–707. https://doi.org/10.1016/j.jmapro.2022.03.056
21. Wang T, Liu H, Dong Z, Ma Y, Sun W, Cui M, Wang X (2023) Laser shock dynamic compaction of tungsten carbide reinforced-aluminum matrix (WCp/Al) composites, J Alloys Compd. 949. https://doi.org/10.1016/j.jallcom.2023.169829
22. Dong Z, Liu HX, Wang T, Ma YJ, Wang X (2022) Three-dimensional multiparticle finite element simulation of dynamic compaction of copper powder by laser shock. Powder Technol. https://doi.org/10.1016/j.powtec.2022.117916
23. Han P, An XZ, Wang DF, Fu H, Yang XH, Zhang H, Zou ZS (2018) MPFEM simulation of compaction densification behavior of Fe-Al composite powders with different size ratios. J Alloys Compd 741:473–481. https://doi.org/10.1016/j.jallcom.2018.01.198
24. Lucht T (2009) Finite element analysis of three dimensional crack growth by the use of a boundary element sub model. Eng Fract Mech 76:2148–2162. https://doi.org/10.1016/j.engfracmech.2009.03.007
25. Fabbro R, Fournier J, Ballard P, Devaux D, Virmont J (1990) Physical study of laser-produced plasma in confined geometry. J Appl Phys 68:775–784. https://doi.org/10.1063/1.346783
26 Hughes TJR, Liu WK, Zimmermann TK (1981) Lagrangian-Eulerian finite element formulation for incompressible viscous flows. Meth Appl Mech Eng 29:329–349. https://doi.org/10.1016/0045-7825(81)90049-9
27 Pagounis E, Lindroos VK (1998) Processing and properties of particulate reinforced steel matrix composites. Mater Sci Eng A 246:221–234. https://doi.org/10.1016/S0921-5093(97)00710-7
28. Sethi G, Myers NS, German RM (2013) An overview of dynamic compaction in powder metallurgy. Int Mater Rev 53:219–234. https://doi.org/10.1179/174328008x309690
29 Nieh TG, Luo P, Nellis W, Lesure D, Benson D (1996) Dynamic compaction of aluminum nanocrystals. Acta Mater 44:3781–3788. https://doi.org/10.1016/1359-6454(96)83816-X
30. Li XJ, Yang WB, Xi JY, Dong SH, Sun M (1999) The lower limit of explosive welding parameter window for bimetal. ExplosMater 28:22–25